Title
Hybrid organic—inorganic solar cells based on bismuth iodide and 1,6-hexanediammonium dication

Journal
Journal of Materials Chemistry A, 4(18)

ISSN
2050-7488

Authors
Fabian, David M
Ardo, Shane

Publication Date
2016

DOI
10.1039/c6ta00517a

Journal of Materials Chemistry A

COMMUNICATION

View Article Online
View Journal | View Issue

Cite this: J. Mater. Chem. A, 2016, 4, 6837

Received 19th January 2016
Accepted 1st March 2016

DOI: 10.1039/c6ta00517a

www.rsc.org/MaterialsA

Hybrid organic–inorganic solar cells based on bismuth iodide and 1,6-hexanediammonium dication†

David M. Fabian[a] and Shane Ardo*[ab]

Heavy metal toxicity and device instability are prominent limitations in the push for commercialization of photovoltaics based on low-cost, solution-processed materials. In this study, a hybrid organic–inorganic material containing trivalent bismuth and dicationic 1,6-hexanediammonium was used as the photoactive layer in solution-processed photovoltaics. These proof-of-concept photovoltaics demonstrated a stable open-circuit photovoltage of 384 ± 12 mV and steady-state short-circuit photocurrent density of 0.101 ± 0.020 mA cm^{-2}. In comparison to the widely studied lead-halide-based perovskites, the bismuth-based materials had superior coverage on mesoporous TiO_2 layers as determined by scanning electron microscopy. Moreover, thermal stability tests demonstrated that these bismuth-based materials were more stable at higher temperatures than comparable lead-based materials.

Introduction

Hybrid organic–inorganic materials have recently garnered increased attention due to the rapid advancement of the light-to-electrical energy conversion efficiency of alkylammonium lead halide perovskite ($APbX_3$) photovoltaics.[1–3] Currently, $APbX_3$-based photovoltaics have demonstrated laboratory efficiencies in excess of 20%.[4,5] $APbX_3$ photovoltaics offer a potential low-cost alternative to established silicon photovoltaic technologies, because most of the components can be deposited from solution using conventional spin-coating methods.[6,7] However, issues with lead toxicity and $APbX_3$ instability remain at the forefront of current research. Lead halides are considered probable carcinogens, and due to their moderate solubility in water, could potentially leach into water supplies, which would deter use of $APbX_3$ photovoltaics.[3] Moreover, alkylammonium halide (AX) dissociates into hydrogen halide and alkylamine which are both particularly volatile, and thus $APbX_3$ degrades to PbX_2 in humid or high-temperature conditions.[8] Lastly, many $APbX_3$ photovoltaic architectures suffer from hysteresis during cyclic voltammetry measurements, which has resulted in inaccurate and typically inflated efficiency values.[3,9] These undesired properties of $APbX_3$ motivate the investigation of a replacement for lead that would allow for equally inexpensive and more environmentally benign photovoltaics, assuming they exhibit similar favorable optoelectronic properties.

$APbX_3$ materials feature a three-dimensional lattice of lead halide that participates in charge-carrier conduction.[10] Small monocationic alkylammonium groups occupy the cavities of the lead iodide lattice and have been suggested to slow charge-carrier recombination.[11] The more general class of hybrid organic–inorganic materials, which range from zero-dimensional to three-dimensional systems, had been investigated for years before intense study began on three-dimensional $APbX_3$-based systems.[12–14] For example, since the late 1990s, bismuth-containing hybrid organic–inorganic materials have shown potential as semiconductors and have been deemed candidates for optoelectronic devices.[13–19] In particular, dicationic alkyldiammonium bismuth halide materials (*e.g.* $HDABiI_5$, where bismuth is in the 3+ oxidation state and HDA is 1,6-hexanediammonium, $[H_3NC_6H_{12}NH_3]^{2+}$) are noteworthy because of reported single-crystal structural resolution, thin-film X-ray diffraction (XRD) patterns that are consistent with preferred crystal orientation, and electronic absorption spectra that suggest an optical bandgap of ~2.0 eV.[13,15] Unlike the three-dimensional lead-halide lattice that forms in $APbX_3$, the bismuth-halide network of dicationic alkyldiammonium bismuth halide materials forms one-dimensional zig-zag chains of distorted BiX_6 octahedra. It has been suggested that the role of the organic groups is to serve as molecular fasteners in these systems.[20] Moreover, Bi^{3+} is the only stable and nontoxic cation with the same $6s^26p^0$ electronic configuration as Pb^{2+}. The favorable electronic properties of $APbX_3$ materials, such as long carrier lifetimes and shallow trap states, are in part due to the electronic contributions of Pb^{2+} to both the conduction band

[a]Department of Chemistry, University of California Irvine, Irvine, CA 92697, USA. E-mail: ardo@uci.edu

[b]Department of Chemical Engineering and Materials Science, University of California Irvine, Irvine, CA 92697, USA

† Electronic supplementary information (ESI) available. See DOI: 10.1039/c6ta00517a

(6p orbitals) and valence band (6s orbitals).[21,22] While Mousdis *et al.* and Mitzi *et al.* have previously synthesized and crystallographically characterized $HDABiI_5$,[13,15] analysis of photovoltaic performance when incorporated as the light absorber in a solar cell has not previously been presented. Recently, $(CH_3NH_3)_3Bi_2I_9$,[23] $Cs_3Bi_2I_9$,[24] and $Cs_2AgBiBr_6$,[22] have been reported as candidate lead-free solar absorbers that were stable in humid air and exhibited excited-state lifetimes on the order of nanoseconds. Those reports, as well as the work disseminated herein, will help spur innovative efforts in bismuth-halide-based hybrid organic–inorganic materials.

Results & discussion

Cross-sectional scanning electron microscopy (SEM) images of a complete $HDABiI_5$ device revealed that the $HDABiI_5$-coated mesoporous TiO_2 nanoparticle layer ($HDABiI_5/mTiO_2$) was 200–250 nm thick (Fig. 1a), which is comparable to the thickness of state-of-the-art mesostructured perovskite solar cells.[25] Top-down SEM images (Fig. S1a†) showed crystal morphology and near-complete surface coverage of $mTiO_2$ by $HDABiI_5$. The majority of $HDABiI_5$ crystal grains appeared to range in size between 200 nm and 400 nm with no preferential orientation in the plane of the deposited film. Also, $HDABiI_5$ covered the $mTiO_2$ to a greater extent than $APbX_3$ processed by the same method (Fig. S1b†). The transmission-mode ultraviolet-visible (UV-Vis) absorption spectrum of an $HDABiI_5$ thin film displayed as Tauc plots are shown in Fig. 1b and c and both suggest that the optical bandgap of $HDABiI_5$ is ~2.1 eV with a lowest-energy indirect transition of 2.05 eV and a lowest-energy direct transition of 2.15 eV. Information on the electronic band structure of $HDABiI_5$ was elucidated from ultraviolet photoemission spectroscopy (UPS) measurements (Fig. S2†). The Fermi level and valence band maximum were measured to be approximately −3.7 eV and −5.6 eV *versus* vacuum, respectively. Considering the calculated optical bandgap of ~2.1 eV (Fig. 1b and c), the conduction band minimum is therefore approximately −3.5 eV *versus* vacuum, signifying that $HDABiI_5$ is an n-type semiconductor (see UPS calculations section in ESI for detailed descriptions and Fig. S3† for the empirical energy-level diagram).

Fig. 2a displays a grazing-incidence XRD pattern of $HDABiI_5$ infiltrated into an $mTiO_2$ layer on top of a $cTiO_2$-coated FTO substrate ($HDABiI_5/mTiO_2/cTiO_2/FTO$). The XRD pattern of the solution-deposited $HDABiI_5$ film matches the pattern determined by Mitzi *et al.* for an $HDABiI_5$ film deposited using a single source thermal ablation technique.[26] $HDABiI_5$ crystallizes in a primitive orthorhombic crystal structure, with lattice constants that match those determined by Mousdis *et al.* for an $HDABiI_5$ single crystal.[13] It is evident from grazing-incidence XRD that the (110) plane is oriented in-plane with the FTO substrate. It is conjectured that the bismuth-iodide chains participate in carrier conduction along the (110) plane, similar to the facilitated carrier conduction along the (110) plane in the lead-halide network of $APbX_3$.[10]

The speciation of the near-surface atoms was characterized by X-ray photoelectron spectroscopy (XPS) (Fig. 2b). Scans of the C 1s core level binding energy revealed the presence of two peaks, corresponding to both C–C and C–N bonds in the organic HDA^{2+} groups.[27] Bi 4f scans indicated that Bi species exist predominantly in the 3+ oxidation state and a small amount as Bi^0, which is suggested to be induced in part during measurement of the XPS spectra (see Explanation for XPS-induced formation of Bi^0 species section and Fig. S4 in ESI†). Ti 2p and O 1s peaks were negligible indicating near-complete coating of $mTiO_2$ by $HDABiI_5$ (see Fig. S5, Table S1, and XPS calculations section in ESI†).

Complete photovoltaic devices with the architecture Au/spiro-OMeTAD/$HDABiI_5/mTiO_2/cTiO_2$/FTO, where spiro-OMeTAD is 2,2′,7,7′-tetrakis(*N*,*N*′-di-*p*-methoxyphenylamine)-9,9′-spirobifluorene, were fabricated and their photovoltaic performances were evaluated (Fig. 3). Current density *versus* potential

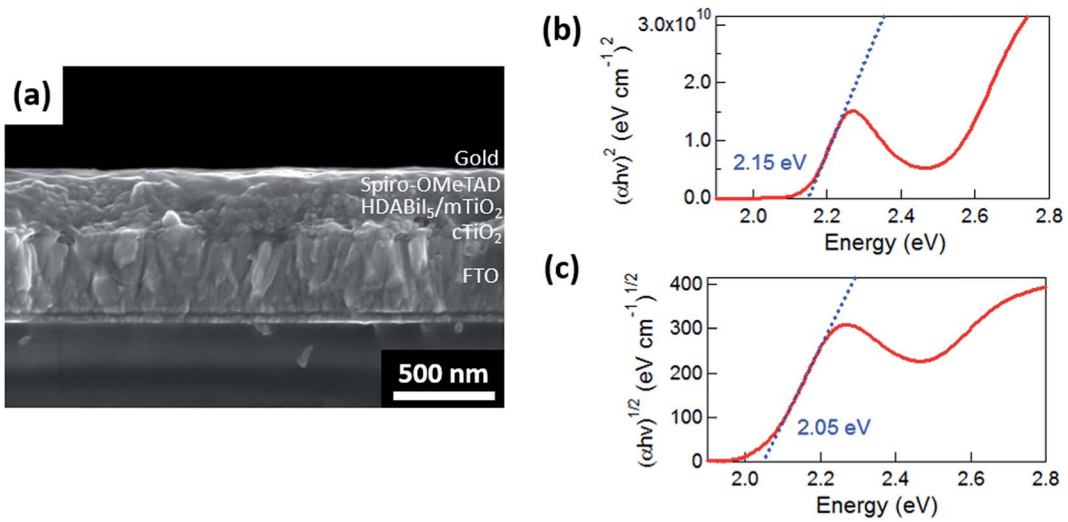

Fig. 1 (a) Cross-sectional scanning electron microscopy image of a representative $HDABiI_5$ device, and (b) direct-bandgap and (c) indirect-bandgap Tauc plots of $HDABiI_5$ deposited as thin films on FTO, baseline corrected for the FTO substrate.

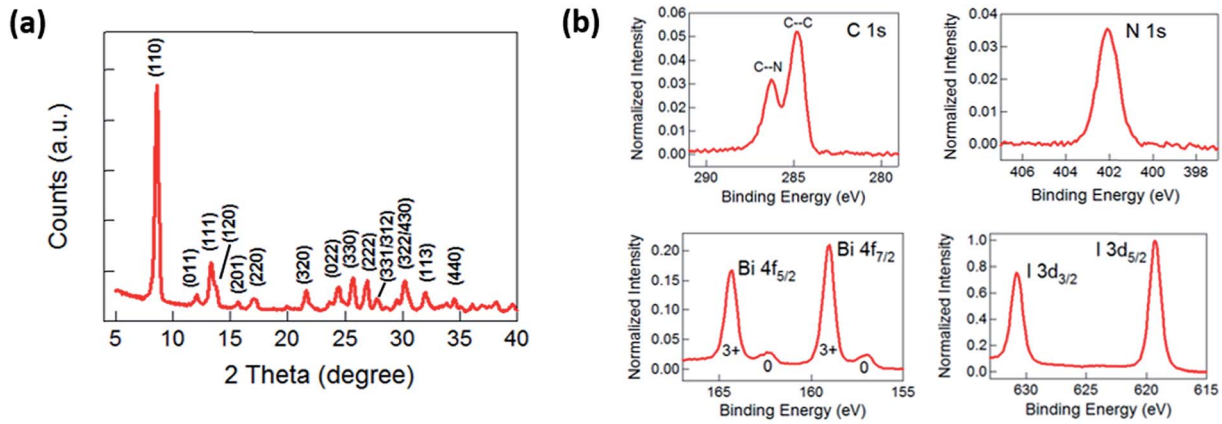

Fig. 2 (a) Grazing-incidence XRD pattern and (b) XPS spectra of $HDABiI_5/mTiO_2/cTiO_2/FTO$, with indicated peak assignments.

(J–E) behavior of a device with an active area of 0.25 cm^2 was measured (Fig. 3a). In the reverse scan direction (indicated by the left-facing arrow), the device exhibited a short-circuit photocurrent density (J_{SC}) of 0.124 mA cm^{-2}, an open-circuit photovoltage (V_{OC}) of 403 mV (384 ± 12 mV over two samples), and a fill factor of 0.43, which yielded a light-to-electrical energy conversion efficiency of 0.027%. The device exhibited a stable steady-state J_{SC} of 0.115 mA cm^{-2} (0.101 ± 0.020 mA cm^{-2} over two samples), as shown in chronoamperometry data (Fig. 3b), which is consistent with the hysteresis observed in the J–E behavior shown in Fig. 3a. The incident-photon-to-current efficiency (IPCE) action spectrum reached a maximum value at 400 nm (Fig. 3c). In the range of 340–450 nm, the $HDABiI_5$ material embedded in the $mTiO_2$ layer converted incident photons to electrical current with >2% external quantum yield (EQY). The non-zero EQY onset at ~600 nm coincides with the absorption onset of the material, and thus supports the calculated optical bandgap of ~2.1 eV. The integrated J_{SC} was determined to be 0.143 mA cm^{-2} (see ESI† for further explanation), which suggests that the illumination intensity used in J–E and chronoamperometry measurements (Fig. 3a and b) was approximately 0.8 Suns. EQY values for $HDABiI_5$ devices were small in comparison to those of state-of-the-art $APbX_3$ devices, for which >80% EQY has been achieved across the spectral region of 400–700 nm.[28] $HDABiI_5$ devices thus require optimization of film thickness, film quality, dopant density, trap-state density, and selective contact engineering to achieve larger J_{SC} values.

Accelerated thermal stability studies were performed on thin films of $HDABiI_5$ as well as $MAPbI_3$ (where MA is methylammonium) perovskites, each deposited on $mTiO_2/cTiO_2/FTO$. Transmission-mode UV-Vis absorption spectra of $HDABiI_5$ thin films were nearly unchanged up to 200 °C, which suggests that there was negligible thermal degradation at this temperature (Fig. 4a). At 300 °C there was noticeable loss in $HDABiI_5$ material noted by a decrease in absorbance; however, there was no significant structural change in the film (*i.e.* features of the absorption spectrum did not change shape and there was no change in film color). This behavior is in contrast to that observed for an $MAPbI_3$ thin film (Fig. 4b) where following treatment at 160 °C (Fig. 4b, red), there was noticeable color change of the film from brown to yellow-brown. By 200 °C (Fig. 4b, green), the film was bright yellow, suggesting a significant loss of MAI and degradation to PbI_2, a semiconductor with a 2.3 eV bandgap (which corresponds to an absorption onset of ~540 nm) (Fig. 4b, inset).[29] These data are consistent with the fact that doubly deprotonated HDA^{2+} of $HDABiI_5$, which is a solid at room temperature and has a boiling point >200 °C, is considerably less volatile than singly deprotonated MA^+ of $MAPbI_3$, which is a gas at room temperature.

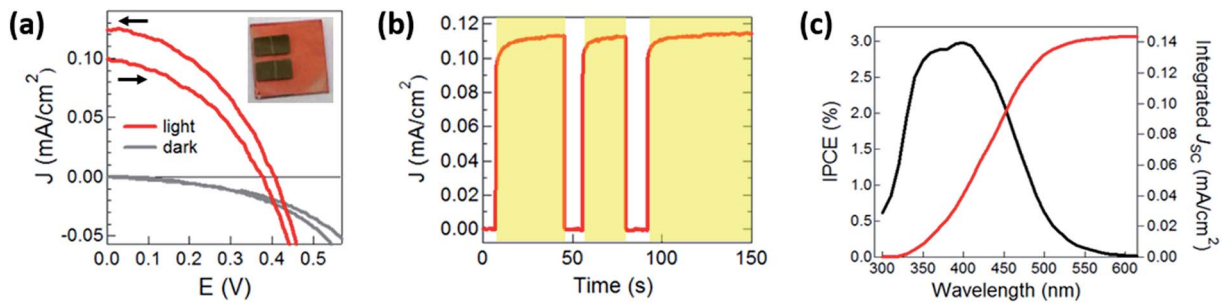

Fig. 3 (a) For a complete Au/spiro-OMeTAD/$HDABiI_5/mTiO_2/cTiO_2/FTO$ device, J–E behavior with scan direction indicated by the arrows and (b) chronoamperometry behavior each under 0.8 Suns illumination, and (c) IPCE action spectrum. Inset in panel (a) is a digital photograph image of the device. Yellow regions in panel (b) indicate time periods of illumination.

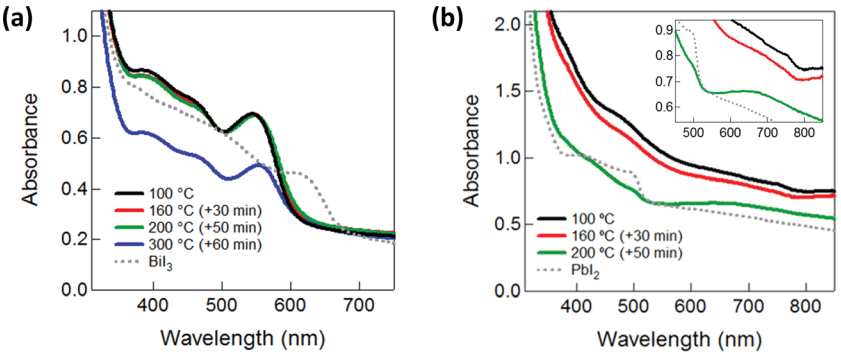

Fig. 4 Transmission-mode UV-Vis electronic absorption spectra at the indicated temperatures (and time beyond 30 minutes of annealing at 100 °C) of (a) $HDABiI_5$ and (b) $MAPbI_3$ films on $mTiO_2/cTiO_2/FTO$. Inset in panel b shows absorption onsets in greater detail and with the same axes units as the main graph.

Conclusions

A hybrid organic–inorganic material, $HDABiI_5$, containing nontoxic bismuth and thermally stable dicationic 1,6-hexanediammonium groups was synthesized and characterized. The electronic absorption spectrum of $HDABiI_5$ was consistent with a material with an optical bandgap of ~2.1 eV. UPS data suggested that the material was n-type. Grazing-incidence XRD data confirmed crystallinity and preferential orientation of $HDABiI_5$. XPS data confirmed the surface elemental composition of $HDABiI_5$ as well as near-complete coverage of the underlying mesoporous TiO_2 nanoparticle layer by $HDABiI_5$. Photoelectrochemical measurements showed that $HDABiI_5$ devices exhibited a steady-state short-circuit photocurrent density of $\sim$100 $\mu A\ cm^{-2}$ and a stable open-circuit photovoltage of almost 400 mV under 0.8 Suns illumination. Thermal stability tests suggested that $HDABiI_5$ is more robust than $MAPbI_3$, which may be attributed to decreased volatility of the deprotonated organic 1,6-hexanediamine group, compared to the deprotonated organic methylamine group of $MAPbI_3$. These results suggest that design of alternative structures with metal valency other than two may allow combinations of organic cationic groups and metal cores necessary for stable and nontoxic solution-processed photovoltaic materials.

Acknowledgements

The authors acknowledge support from the Department of Chemistry and the School of Physical Sciences at the University of California, Irvine. D. M. F. acknowledges support by the National Science Foundation Graduate Research Fellowship under Grant No. DGE-1321846. XPS and UPS work was performed at the UC Irvine Materials Research Institute (IMRI) using instrumentation funded in part by the National Science Foundation Major Research Instrumentation Program under Grant No. CHE-1338173. The authors thank Dr. Ich Tran (UC Irvine) for guidance in XPS and UPS data analysis and Prof. Ron Grimm (Worcester Polytechnic Institute) for guidance in XPS data analysis. The authors also thank group members of the laboratory of Prof. Matt Law (UC Irvine) for providing training and access to their O_2 plasma cleaner, thermal evaporator, and IPCE setup.

References

1 T. C. Sum and N. Mathews, *Energy Environ. Sci.*, 2014, **7**, 2518–2534.
2 M. A. Green, A. Ho-Baillie and H. J. Snaith, *Nat. Photonics*, 2014, **8**, 506–514.
3 M. Grätzel, *Nat. Mater.*, 2014, **13**, 838–842.
4 W. S. Yang, J. H. Noh, N. J. Jeon, Y. C. Kim, S. Ryu, J. Seo and S. I. Seok, *Science*, 2015, **348**, 1234–1237.
5 D. Bi, W. Tress, M. I. Dar, P. Gao, J. Luo, C. Renevier, K. Schenk, A. Abate, F. Giordano, J. C. Baena, J. Decoppet, S. M. Zakeeruddin, M. K. Nazeeruddin, M. Grätzel and A. Hagfeldt, *Sci. Adv.*, 2016, **2**, e1501170.
6 J. Burschka, N. Pellet, S.-J. Moon, R. Humphry-Baker, P. Gao, M. K. Nazeeruddin and M. Grätzel, *Nature*, 2013, **499**, 316–319.
7 S. D. Stranks, G. E. Eperon, G. Grancini, C. Menelaou, M. J. P. Alcocer, T. Leijtens, L. M. Herz, A. Petrozza and H. J. Snaith, *Science*, 2013, **342**, 341–344.
8 J. M. Frost, K. T. Butler, F. Brivio, C. H. Hendon, M. van Schilfgaarde and A. Walsh, *Nano Lett.*, 2014, **14**, 2584–2590.
9 H. J. Snaith, A. Abate, J. M. Ball, G. E. Eperon, T. Leijtens, N. K. Noel, S. D. Stranks, J. T. Wang, K. Wojciechowski and W. Zhang, *J. Phys. Chem. Lett.*, 2014, **5**, 1511–1515.
10 A. Ishii, A. K. Jena and T. Miyasaka, *APL Mater.*, 2014, **2**, 091102.
11 C. Motta, F. El-Mellouhi, S. Kais, N. Tabet, F. Alharbi and S. Sanvito, *Nat. Commun.*, 2015, **6**, 7026.
12 G. C. Papavassiliou, *Prog. Solid State Chem.*, 1997, **25**, 125–270.
13 G. A. Mousdis, G. C. Papavassiliou, A. Terzis and C. P. Raptopoulou, *Z. Naturforsch., B: J. Chem. Sci.*, 1998, **53**, 927–931.
14 D. B. Mitzi, *Inorg. Chem.*, 2000, **39**, 6107–6113.
15 D. B. Mitzi and P. Brock, *Inorg. Chem.*, 2001, **40**, 2096–2104.
16 M. Lindsjö, A. Fischer and L. Kloo, *Z. Anorg. Allg. Chem.*, 2005, **631**, 1497–1501.

17 C. Hrizi, A. Samet, Y. Abid, S. Chaabouni, M. Fliyou and A. Koumina, *J. Mol. Struct.*, 2011, **992**, 96–101.
18 C. Hrizi, A. Trigui, Y. Abid, N. Chniba-Boudjada, P. Bordet and S. Chaabouni, *J. Solid State Chem.*, 2011, **184**, 3336–3344.
19 C. Hrizi, N. Chaari, Y. Abid, N. Chniba-Boudjada and S. Chaabouni, *Polyhedron*, 2012, **46**, 41–46.
20 T. Kodzasa, H. Ushijima, H. Matsuda and T. Kamata, *Mol. Cryst. Liq. Cryst. Sci. Technol., Sect. A*, 2000, **343**, 71–75.
21 T. Umebayashi, K. Asai, T. Kondo and A. Nakao, *Phys. Rev. B: Condens. Matter Mater. Phys.*, 2003, **67**, 155405.
22 A. H. Slavney, T. Hu, A. M. Lindenberg and H. I. Karunadasa, *J. Am. Chem. Soc.*, 2016, **138**, 2138–2141.
23 R. Hoye, R. E. Brandt, A. Osherov, V. Stevanovic, S. D. Stranks, M. W. B. Wilson, H. Kim, A. J. Akey, R. C. Kurchin, J. R. Poindexter, E. N. Wang, M. G. Bawendi, V. Bulovic and T. Buonassisi, *Chem. - Eur. J.*, 2016, **22**, 2605–2610.
24 B.-W. Park, B. Philippe, X. Zhang, H. Rensmo, G. Boschloo and E. M. J. Johansson, *Adv. Mater.*, 2015, **27**, 6806–6813.
25 T. Salim, S. Sun, Y. Abe, A. Krishna, A. C. Grimsdale and Y. M. Lam, *J. Mater. Chem. A*, 2015, **3**, 8943–8969.
26 D. B. Mitzi, M. T. Prikas and K. Chondroudis, *Chem. Mater.*, 1999, **11**, 542–544.
27 J. F. Moulder, W. F. Stickle, P. E. Sobol and K. D. Bomben, *Handbook of X-ray Photoelectron Spectroscopy*, 1995, p. 261.
28 M. Xiao, F. Huang, W. Huang, Y. Dkhissi, Y. Zhu, J. Etheridge, A. Gray-Weale, U. Bach, Y.-B. Cheng and L. Spiccia, *Angew. Chem., Int. Ed.*, 2014, **126**, 10056–10061.
29 A. Ferreira da Silva, N. Veissid, C. Y. An, I. Pepe, N. Barros de Oliveira and A. V. Batista da Silva, *Appl. Phys. Lett.*, 1996, **69**, 1930.